Journal of Cosmetics, Dermatological Sciences and Applications, 2026, 16(3), 200-221
https://www.scirp.org/journal/jcdsa
ISSN Online: 2161-4512
ISSN Print: 2161-4105

Dual Protection against Photoaging and Pollution-Induced Skin Damage through Multi-Level Antioxidant and Reparative Mechanisms

Jing Wang[1,2*], Mauricio Valerio-Santiago[3*], Minjia Yuan[1,2], Qi Li[1,2], Consuelo García[3], Gemma Mola[3], Eva Gómez[3], Melanie Qiao[4], Juan Cebrián[3], Cuicui Zhu[1,2#]

[1]Shanghai Qiran Biotechnology Co., Ltd., Shanghai, China
[2]Shanghai Jinjia Technology Co., Ltd., Shanghai, China
[3]Lubrizol Life Science, Lipotec S.A.U., Barcelona, Spain
[4]Lubrizol Specialty Chemicals (Shanghai) Co., Ltd., Shanghai, China
Email: wangjing4118@163.com, Mauricio.Valerio@Lubrizol.com, #zhucuicui@outlook.com

How to cite this paper: Wang, J., Valerio-Santiago, M., Yuan, M.J., Li, Q., García, C., Mola, G., Gómez, E., Qiao, M., Cebrián, J. and Zhu, C.C. (2026) Dual Protection against Photoaging and Pollution-Induced Skin Damage through Multi-Level Antioxidant and Reparative Mechanisms. *Journal of Cosmetics, Dermatological Sciences and Applications*, **16**, 200-221.
https://doi.org/10.4236/jcdsa.2026.163014

Received: June 30, 2026
Accepted: August 30, 2026
Published: September 2, 2026

Abstract

Objective: Environmental factors like ultraviolet (UV) radiation and air pollution accelerate extrinsic skin aging by inducing reactive oxygen species (ROS), leading to oxidative stress and cellular damage. This study investigated the protective potential of Dimethylmethoxy Chromanol (DMMC) and *Vigna angularis* seed extract, both unpreserved (AZK) and preserved (XPO) forms, individually and in combination, using *in vitro*, *ex vivo*, and clinical evaluations. **Methods:** Primary human skin cells and pigmented skin equivalents were exposed to UVA/UVB, H_2O_2, or $PM_{2.5}$. Assessments included immunofluorescence, protein carbonylation, malondialdehyde (MDA) quantification, comet assays, and LC-MS/MS analysis for oxidative DNA/RNA lesions. Transcriptomic profiling analyzed DMMC-induced gene expression. A 28-day, randomized, double-blind, placebo-controlled clinical hemi-face study (n = 33) assessed wrinkle reduction via PRIMOS 3D imaging. **Results:** AZK rapidly reduced oxidative DNA/RNA lesions in keratinocytes under combined stressors. DMMC exerted a dual mechanism: direct radical scavenging and transcriptional activation of antioxidant, detoxification, and efflux genes. It protected against pyrene/UVA genotoxicity, UVB-induced protein oxidation, and H_2O_2 cytotoxicity. In pigmented skin models, co-treatment with XPO and DMMC further elevated loricrin, Ki67, and COL VII levels relative to XPO.

*Co-first authors.
#Corresponding author.

monotherapy, while reducing protein carbonylation and lipid peroxidation. Clinically, the combined formulation significantly reduced wrinkle depth at day 28 compared to placebo. **Conclusion:** DMMC and *Vigna angularis* Seed Extract provide complementary protection against environmental skin stress. AZK offers rapid antioxidative defense, while DMMC bolsters acute and long-term cellular resilience. Their combination restores epidermal structural integrity in *ex vivo* skin models and relieves facial wrinkling in human clinical testing, supporting their application in anti-photoaging skincare formulations.

Keywords

DMMC, XPO, AZK, Photoaging, Skin Protection, Pollution-Induced Damage

1. Introduction

The skin, serving as the body's primary barrier and outermost interface with the environment, is continually exposed to ultraviolet (UV) radiation, air pollutants, and reactive oxygen species (ROS). These stressors lead to a cascade of damaging events including lipid peroxidation, protein oxidation, DNA damage, melanogenesis, and cellular dysfunction, all of which contribute to premature aging and pigmentation disorders [1]-[5].

UVA (320 - 400 nm) and UVB (280 - 320 nm) radiation are well-known inducers of photo-oxidative stress, promoting the generation of ROS such as superoxide anion, hydroxyl radicals, and singlet oxygen [6] [7]. These species trigger the accumulation of malondialdehyde (MDA) and carbonylated proteins, which serve as biomarkers for lipid and protein oxidation, respectively [8] [9]. Moreover, UV exposure stimulates melanogenesis, leading to pigmentary changes. At the genomic level, UV and pollutant exposure induce oxidative DNA damage, including the formation of 8-oxo-7,8-dihydro-2'-deoxyguanosine (8-oxodG), 8-hydroxyguanosine (8-OHG), and DNA strand breaks [6] [10] [11]. Additionally, hydrogen peroxide (H_2O_2), commonly used as a model of oxidative stress, induces cytotoxic effects, serving as a valuable tool for evaluating the protective potential of antioxidant compounds *in vitro* [12].

To mitigate such multifactorial damage, novel multifunctional cosmetic ingredients are being developed to reinforce the skin's antioxidant defenses and repair capacity. In this context, Lipochroman™ molecule (Dimethylmethoxy Chromanol, DMMC) and Xpozuki™ biotech ingredient (XPO, containing *Vigna angularis* seed extract) represent two promising actives with complementary mechanisms of action.

DMMC is a potent synthetic antioxidant widely used in cosmetic formulations. Structurally, it closely resembles γ-tocopherol, the classical form of vitamin E, which is renowned for its ability to scavenge free radicals and quench singlet oxygen ($^1O_2$). This structural similarity is functionally significant, as $^1O_2$ is a key re-

active oxygen species generated in the skin following UVA exposure and is a major contributor to photooxidative damage [13]. The ability of DMMC to quench singlet oxygen has been demonstrated both in solution and in an *ex vivo* skin model [14]. Furthermore, DMMC's antioxidant efficacy has been validated in interlaboratory studies comparing its performance to that of other known antioxidants.

Mechanistically, DMMC also exerts strong anti-nitrosative effects by efficiently neutralizing peroxynitrite ($ONOO^-$), a highly reactive nitrogen species involved in nitrosative stress. This activity is attributed to a key structural feature—a substitution at position 5 on the chromanol ring—which enables the selective and effective capture of $ONOO^-$.

XPO is a preserved form of *Vigna angularis* seed extract (AZK) in solution, where the extract has been obtained by means of biotechnology from *Vigna angularis* seeds. *Vigna angularis* seed extract offers documented antioxidant and anti-photoaging benefits, helping protect the skin from UVB-induced oxidative damage and extracellular matrix degradation [15].

In the present study, we systematically assessed the protective and restorative efficacy of DMMC and *Vigna angularis* seed extract, either in AZK or XPO, individually and in combination, against various models of oxidative stress in skin cells. Specifically, we evaluated their ability to counteract UVA/UVB-induced lipid and protein oxidation, melanogenesis, DNA strand breaks and nucleic acid oxidative lesions (8-OHG and 8-oxodG) under photooxidative and environmental stress conditions, as well as H_2O_2-induced cytotoxicity. Our findings aim to provide mechanistic insight into how these ingredients can contribute to skin protection in cosmetic formulations targeting urban skin stress.

2. Materials and Methods

2.1. Test Compounds

AZK is the unpreserved *Vigna angularis* seed extract obtained by biotechnology, and Xpozuki™ biotech ingredient (XPO) is the preserved, in-solution form of the same extract, AZK, XPO and Lipochroman™ molecule (DMMC; Dimethylmethoxy Chromanol) are provided by Lubrizol Life Science (Gavà, Spain). Xpozuki™ and Lipochroman™ are trademarks of The Lubrizol Corporation or its affiliates.

AZK concentrations (44 and 88 μg/mL) are calculated based on active solid content of the raw botanical extract, while XPO dosages are presented as weight percentages of the finished stock formulation as received from the manufacturer.

DMMC was tested at two distinct concentrations according to separate experimental models, due to the different exposure systems and testing purposes. For *ex vivo* 3D reconstructed pigmented skin equivalent assays, the combined treatment contained 0.005% DMMC mixed with 2% XPO for topical application on tissue constructs. And for the 28-day clinical hemi-face trial formulation, DMMC was incorporated at 0.05% together with 2% XPO in the topical cream for human skin use.

2.2. Cells and Culture

Primary human adult epidermal keratinocytes (HEKa, Cat. No. C-005-5C), melanocytes (HEM, Cat. No. C-002-25), and human dermal fibroblasts (HDF, Cat. No. C-013-5C) were purchased from Thermo Fisher Scientific. All cells were used at passages P3-P6, cultured at 37˚C with 5% CO_2 in their respective manufacturer-supplied serum-free media.

2.3. 3D Reconstructed Pigmented Skin Equivalent Model

Full-thickness pigmented skin equivalents were reconstructed in-house following well-documented organotypic skin culture protocols. Dermal equivalents were created by seeding human dermal fibroblasts (HDF) into a collagen matrix and culturing them for 10 days under submerged conditions to support ECM formation. On Day 12, active compounds were added to the culture medium. On Day 21, human epidermal keratinocytes (HEKa) and melanocytes (HEM) were seeded on the matured dermal, then cultured at an air-liquid interface to induce stratification and melanogenesis until Day 28, with 20 additional days of maturation.

Between Days 46 - 48, constructs were exposed to standardized UVA (16 J/cm^2) and UVB (100 mJ/cm^2) irradiation to simulate solar damage. Post-irradiation, samples were collected for histological, molecular, and biochemical analyses.

2.4. Hematoxylin-Phloxine-Saffron (HPS) Staining

5 µm paraffin section of 3D pigmented skin equivalent were baked at 60˚C for 1 - 2 h, then deparaffinization in xylene (2 changes, 5 min each) and rehydration through graded alcohols. Then rinsed in running tap water. Sections were stained in hematoxylin for 5 min, differentiated in 1% acid alcohol (1 - 2 dips), and blued in ammonia water for 1 min (5 min tap water rinses after each step). Cytoplasmic staining was done in phloxine for 2 min, rinsed, differentiated and dehydrated in 95% ethanol, and dehydrated thoroughly in absolute ethanol (3 - 4 changes). Then stained in saffron solution for 5 min. finally, sections were dehydrated in absolute ethanol (3 changes), cleared in xylene (2 changes, 3 min each), and mounted with a resinous mounting medium. Nine representative images per condition were captured using an Axioskop 2 Plus optical microscope (Zeiss), DS-Ri1 CCD camera (Nikon) and NIS-Elements software (Nikon).

2.5. Warthin Starry Staining

After deparaffinization and rehydration, skin sections were incubated with a silver nitrate solution at 6% for 20 min following Suppliers' kit instruction (Merck). The development of the silver was stopped in a washing step with water. Then, skin sections were incubated with hydroquinone and gelatin mixture. This step allowed the development of melanin granules in dark brown to black and the counterstaining of skin equivalent sections in yellow to orange. Image acquisition was identical to HPS staining.

2.6. Immunohistological Assay

Paraffin sections underwent heat-mediated antigen retrieval and were blocked with PBS containing 4% BSA for 30 min at room temperature. Sections were incubated overnight with primary antibodies targeting markers of barrier function (loricrin, LOR, Abcam), proliferation (Ki67, Dako), ECM structure (type VII collagen, COL VII, Santa Cruz), and oxidative stress (Carbonylation and MDA, Genetex). The following day, sections were incubated for 1 h in the dark with AlexaFluor-568-conjugated anti-mouse or anti-rabbit secondary antibodies (Molecular Probes, Invitrogen). Nuclear counterstaining was performed with DAPI. Negative controls were prepared using isotype-matched IgG.

16-bit TIFF images (3 fields/sample) were acquired with a Zeiss Axio Observer D1 microscope (n = 9). Positive signal areas were segmented, quantified, and normalized to the dermal-epidermal junction (DEJ) length (for LOR, Ki67, COL VII and MDA) or the dermal region (for carbonylation), and expressed as the percentage of positive signal density.

2.7. Environmental Stressors-Induced DNA/RNA Damage Assessment (8-oxodG/8-OHG)

HEKa cells (2×10^5 cells/well) were seeded in 6-well plates and pretreatments with AZK (44 or 88 μg/mL) for 1 h, while controls received medium only. Cells were exposed to a simulated greenhouse effect (38˚C in 20% CO_2, overnight), then $PM_{2.5}$ (2.34 μg/cm^2) in phosphate-buffered saline (PBS) and solar-simulated irradiation (12.15 - 36 J/cm^2). DNA and RNA was extracted (QIAGEN DNeasy Kit, QIAcube), quantified (NanoDrop), and enzymatically hydrolyzed. 8-oxodG and 8-OHG was performed by LC-MS/MS (Shimadzu LCMS-8040, EC-C18 column) with gradient elution. MRM transitions for 8-oxodG (m/z 284.15 > 168.05, confirmatory 140.1) and 8-OHG (m/z 300.00 > 168.05, confirmatory 140.05) were monitored. Protective effects of AZK were calculated using the established formula.

2.8. Transcriptomic Profiling (Microarray)

Microarray detection and bioinformatic analysis were performed by Bioarray S.L. Spain. Custom Agilent 8 × 44 K two color microarrays with ID 014850 were used following Agilent two color labeling protocol version 6.5. HEKa cells (2×10^5 cells/well, 6-well plates) were treated with 50 μg/mL DMMC in 0.14% ethanol for 16 - 24 h; controls received ethanol vehicle only. RNA was extracted (RNeasy Plus Mini Kit) and labeling followed Agilent's Two-Color protocol (Cy3/Cy5, n = 2) for microarray. All statistical analysis was carried with Bioconductor, with de packages for microarray analysis Limma, Marray, affy, pcaMethods, RankProd and EMA, under R environment. Genes for functional enrichment satisfied $|\log_2 FC| > 1$ and adjusted p value < 0.05 simultaneously.

2.9. Alkaline Comet Assay for DNA Damage

HEKa cells (Pyrene + UVA/Visible Light)

HEKa cells were treated with DMMC at concentrations of 30 or 50 μg/mL, with or without pyrene at 3 or 4 μM for 2 h, then irradiated with UVA/visible light (The total irradiation dose was 45 kJ/m^2, delivered over 69 s at an irradiance of 650 W/m^2, CPS+ solar simulator, 4˚C). Cells were embedded in low-melting-point agarose (LMPA) on precoated slides, then lysed in 4˚C for 90 min, subjected to alkaline unwinding 20 min at 25˚C, followed by electrophoresis for 20 min at 25 V and 300 Ma, neutralized, and dehydrated. Stained with ethidium bromide, 100 cells/sample were imaged (Olympus, BX53-RFL) and analyzed using Komet software (version 6.0) for Olive Tail Moment (OTM). χ^2 OTM was calculated via non-linear regression, and DNA protection (%Pr) via the established formula.

Human Melanocytes (UV Irradiation)

Melanocytes were incubated with DMMC at concentrations of 1, 10, or 50 μg/mL in culture medium for 2 h at 37˚C, then irradiation with UVB (The UVB lamp delivered a calibrated 312 nm beam at an intensity of 0.91 mW/cm^2, yielding a total dose of 0.06 J/cm^2 with 1 min irradiation) or UVA (The UVA lamp delivered a 365 nm beam at 4 mW/cm^2, corresponding to a total dose of 1.0 J/cm^2 with 4.2 min exposure). Comet assay, OTM/χ^2 OTM quantification, and %Pr calculation were identical to HEKa cell procedures.

2.10. H_2O_2-Induced Cytotoxicity Assay

Human dermal fibroblasts (2×10^4 cells/well, 96-well plates) were pretreated with DMMC for 30 min, followed by exposure to 735 μM H_2O_2 (Sigma) for 24 h. Cell viability was assessed using the Calcein-AM assay (Molecular Probes), with representative images from Neutral Red Uptake staining.

2.11. Cellular Protein Carbonyl Assay

Human dermal fibroblast (5×10^4 cells/well, 24-well plates) were treated with DMMC (0.5, 1, or 10 μg/mL) for 24 h, then irradiated with UVB (17.592 W/m^2 for 5 min, total dose 0.52 J/cm^2) on a cool tray. After 1 h incubated in fresh medium, cells were washed, lysed, and subjected to nucleic acid removal. Protein concentrations were measured determined by BCA assay and samples were diluted to 10 μg/mL. Carbonylated proteins were quantified using the Protein Carbonyl ELISA Kit (Cell Biolabs) with a BSA standard curve for absolute quantification.

2.12. Cellular Melanogenesis Evaluation

Human melanocytes (5×10^5 cells/well, 6-well plates) were treated with DMMC, with controls receiving medium alone. After 4 days, cells were harvested, counted, and lysed in 1 mL of 1 N NaOH with 10% DMSO for 2 h at 80˚C. After centrifugation, melanin content was measured at 450 nm (Tecan Genios) and quantified using a synthetic melanin standard curve, expressed as pg/cell and percentage of control.

2.13. Clinical Hemi-Face Study

A double-blind, placebo-controlled, 28-day clinical hemi-face study was performed with 33 healthy women aged 45 - 60 years with dull, sallow skin with visible with crow's feet region. Random side allocation was implemented at baseline to assign the test cream containing 2% XPO and 0.05% DMMC or matching placebo cream to either the left or right facial half of each volunteer. Identical texture, colour and fragrance were used for both formulations to maintain blinding status for all participants, product applicators and instrumental assessors throughout the trial. No subjects withdrew from the full 28-day treatment period. All volunteers acted as their own internal control, and all instrumental data were statistically analysed using paired comparison methods. Test and placebo creams were applied twice daily to the allocated contralateral facial sides. Skin efficacy parameters including fine lines, wrinkles, texture, pigmentation and UV spots were quantified via Antera®3D, PRIMOS and VISIA CR image analysis systems. The study was conducted in accordance with the Declaration of Helsinki and written informed consent was obtained from all participants before enrolment.

2.14. Statistical Analysis

Data are presented as mean ± SEM/SD with biological/technical replicates specified per assay. n now explicitly refers to independent biological replicates (independent cultures or constructs), except for the immunohistological quantification, where n = 9 corresponds to 3 randomly selected fields from each of 3 independent constructs; this is now stated as "3 fields × 3 constructs" to remove any ambiguity.

Statistical significance was determined as follows:

One-way/unpaired Student's *t*-test: most *in vitro* assays (*$p < 0.05$, *$p < 0.01$, **$p < 0.001$, ***$p < 0.0001$);

One-way ANOVA: 8-oxodG/8-OHG assay (same p thresholds);

Shapiro-Wilk test + Student's *t*-test/Wilcoxon test: clinical study (normality verification first);

χ^2 test + Student's *t*-test: comet assay (χ^2 OTM calculation and group comparison).

3. Results

3.1. XPO Alleviates UV-Induced Melanogenesis in 3D Pigmented Skin and DNA Damage Induced by Combined Stressors in HEKa

The protective efficacy of XPO or its preservative-free version AZK was evaluated using two complementary models: UV irradiated 3D reconstructed pigmented skin, and HEKa cells exposed to combined environmental stressors, such as CO_2, $PM_{2.5}$, and solar-simulated irradiation.

In the 3D skin model, Warthin Starry staining showed that UV exposure resulted in marked melanin accumulation throughout the epidermis, while topical

application of 2% XPO (day 12 - 46) visibly reduced pigmentation, suggesting an inhibitory effect on UV-stimulated melanogenesis (Figure 1(A)). In HEKa cells, combined stressors significantly elevated genomic damage markers including 8-oxodG and 8-OHG levels, while treated with AZK (44 and 88 μg/mL) reduced these levels (Figure 1(B), Figure 1(C)).

Collectively, XPO provides multi-level protection against environmentally induced skin damage. It attenuates UV-induced melanogenesis in reconstructed pigmented skin and preserves genomic integrity in keratinocytes under combined climate, pollution, and solar stress.

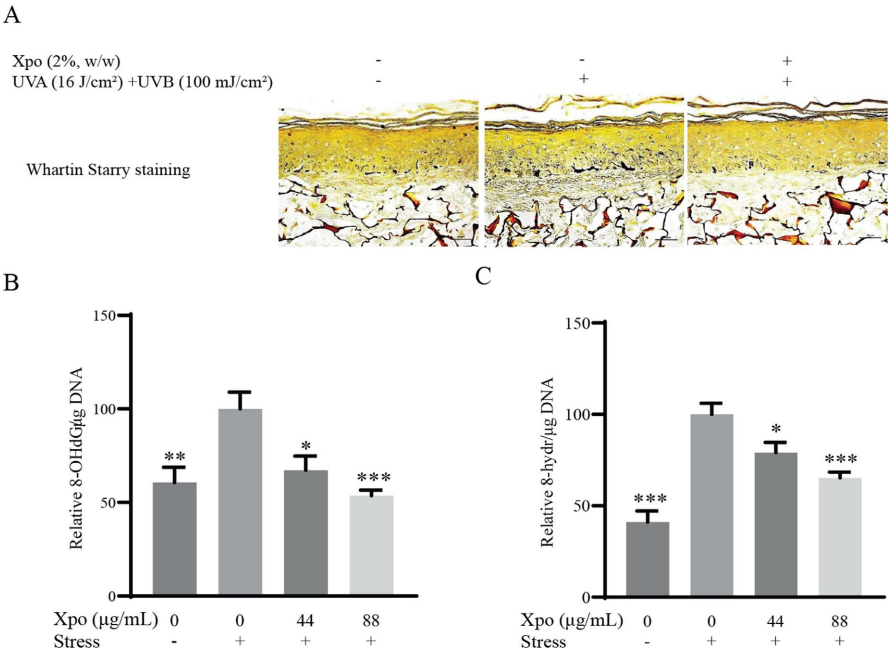

Figure 1. Effects of XPO on UV-induced pigmentation in reconstructed pigmented human skin model and of AZK on DNA/RNA damage in HEKa exposed to combined stressors. (A) Histological analysis of a 3D reconstructed pigmented skin model following UVA (16 J/cm²) and UVB (100 mJ/cm²) exposure, with or without topical application of 2% XPO from day 12 to day 46 of culture. Warthin Starry staining shows melanin distribution in the epidermis. (B) (C) Quantification of 8-oxodG (B) and 8-OHG (C) levels in HEKa cells pretreated with AZK (44 or 88 μg/mL) under combined stressors: greenhouse-like conditions (38˚C, 20% CO_2), followed by exposure to $PM_{2.5}$ (2.34 μg/cm²) and solar-simulated irradiation (12.15 - 36 J/cm²). Data are presented as mean ± SEM (n = 5 for (B) (C)). *p < 0.05, **p < 0.01, ***p < 0.001 and ****p < 0.0001 versus UV-irradiated or stressed controls. Scale bar = 50 μm.

3.2. DMMC Activates Antioxidant, Detoxification, and Barrier-Related Gene Networks in HEKa

To investigate DMMC's effect on gene expression, transcriptomic profiling was performed in HEKa cells treated with 50 μg/mL DMMC for 16 - 24 h. Gene expression analysis revealed that DMMC significantly upregulated genes associated with epidermal barrier formation, antioxidant redox homeostasis, and xenobiotic metabolism/efflux in keratinocytes, which collectively enhanced the skin's struc-

tural resilience and defense capacity against environmental stress. Specifically, the small proline-rich protein (SPRR) family genes (key for cornified envelope formation and oxidative stress adaptation [16] [17]) were markedly induced; core antioxidant genes involved in glutathione metabolism and free radical scavenging were highly upregulated; and phase I/II detoxification as well as cellular efflux transporter genes were activated, indicating DMMC exerts multi-dimensional protective effects via transcriptional regulation (**Appendix** Table A2).

3.3. DMMC Protects Human Skin Cells from Oxidative and Genotoxic Stress and Suppresses Basal Melanogenesis

To validate the functional consequences of DMMC-induced transcriptional changes, a series of *in vitro* assays were performed to evaluate its protective effects against oxidative and genotoxic stress, as well as suppress melanogenesis in human skin cells (keratinocytes, melanocytes, fibroblasts). The results showed that DMMC exerts multi-faceted protective effects on skin cells through dose-dependent regulation.

In HEKa cells, single treatment with UVA/visible light (4.5 J/cm^2), pyrene (3 or 4 μM) or DMMC (30 or 50 μg/mL) did not induce significant DNA damage, while the combined exposure of irradiation and pyrene induced DNA damage with increase in OTM/χ^2 OTM values. However, pretreated with DMMC significantly mitigated pyrene-induced DNA damage (**Figure 2(A)**), effectively counteracting UVA and pollution induced genotoxic stress in keratinocytes. In human melanocytes, pretreated with DMMC (1, 10, or 50 μg/mL) visibly attenuated UVA (1.00 J/cm^2) induced DNA damage, particularly at 10 and 50 μg/mL, while offering no apparent protection against UVB (0.06 J/cm^2) induced DNA damage (**Figure 2(B)**), reflecting the wavelength specificity of its photoprotective effect on DNA.

For fibroblasts (HDFs), DMMC displayed antioxidant and cytoprotective effect. Pretreated with DMMC attenuated H_2O_2 (735 μM) induced oxidative cytotoxicity, with 1 μg/mL DMMC significantly restoring cell viability, improving cellular adherence, and preserving structural integrity of HDFs (**Figure 2(C)**). Additionally, DMMC (0.5, 1, or 10 μg/mL) mitigated UVB (0.52 J/cm^2) induced protein oxidative damage in HDFs. UVB irradiation significantly elevated protein carbonyl levels compared to non-irradiated controls, while DMMC pretreatment led to a dose-dependent reduction in protein carbonylation. A significant decrease was observed at 0.5 μg/mL, with further reductions at 1 and 10 μg/mL, demonstrating the efficacy of DMMC in mitigating UVB-induced protein oxidation (**Figure 2(D)**). Furthermore, DMMC exhibited a notable inhibitory effect on melanogenesis in melanocytes. DMMC treatment significantly reduced melanin levels relative to untreated controls and visibly diminished pigmentation, supporting its potential value for ameliorating hyperpigmentation and uneven skin tone (**Figure 2(E)**).

Overall, these *in vitro* findings confirm that DMMC can protect multiple types of human skin cells from oxidative stress through dose-dependent regulation,

with unique wavelength specificity in photoprotection, and also effectively suppress melanogenesis, collectively demonstrating its dimensional protective activity on skin tissue.

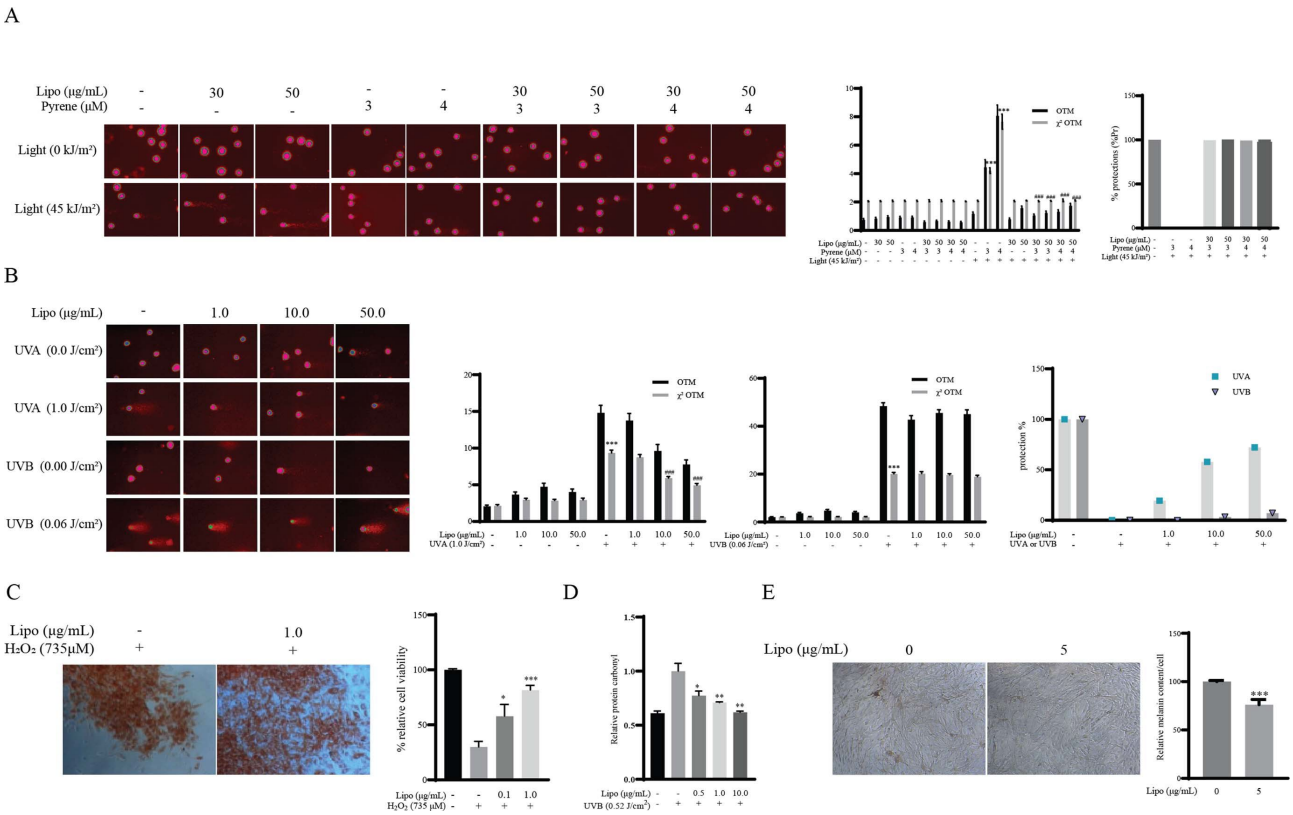

Figure 2. Effects of DMMC on DNA damage, oxidative stress, and melanogenesis. (A) (B) Human keratinocytes (A) and melanocytes (B) pretreated with DMMC at the indicated concentrations and exposed to either phototoxic stress (pyrene + UVA/visible light, 4.5 J/cm^2) or UV radiation (UVA, 1.0 J/cm^2 or UVB, 0.06 J/cm^2). DNA strand breaks assessed using the alkaline comet assay and quantified by OTM and χ^2 OTM. For each condition, 100 cells were analyzed (50 cells per slide). χ^2 OTM values were derived by nonlinear regression of normalized OTM distributions. (C) HDFs pretreated with DMMC (0.1 or 1 μg/mL) prior to H_2O_2 (735 μM) exposure. Cell viability evaluated using the Calcein-AM assay and visualized using neutral red uptake staining. Data represent mean ± SD (n = 3); *p < 0.05, ****p < 0.0001 vs. H_2O_2-only group. (D) HDFs pretreated with DMMC (0.1, 1 or 10 μg/mL) prior to UVB (0.52 J/cm^2) exposure. Carbonylated protein content quantified using Protein Carbonyl ELISA kit and expressed as mean ± SD (n = 4); *p < 0.05, **p < 0.01 vs. UVB-only control. (E) Melanocytes treated with DMMC (5.0 μg/mL), and melanin content was measured by absorbance and normalized to cell number. Results are expressed as percentage relative to untreated controls (mean ± SEM, n = 3); ****p < 0.0001 vs. control.

3.4. Combined Treatment with XPO and DMMC Alleviates UV-Induced Oxidative Stress and Improves Epidermal Homeostasis in 3D Reconstructed Pigmented Human Skin Model

To compare the individual and combined protective effects of XPO and DMMC under UV-induced skin damage, a 3D reconstructed pigmented human skin model was subjected to combined UVA (16 J/cm^2) and UVB (100 mJ/cm^2) irradiation, with HPS staining confirming intact epidermal and dermal reconstruction in all groups (Figure 3(C)).

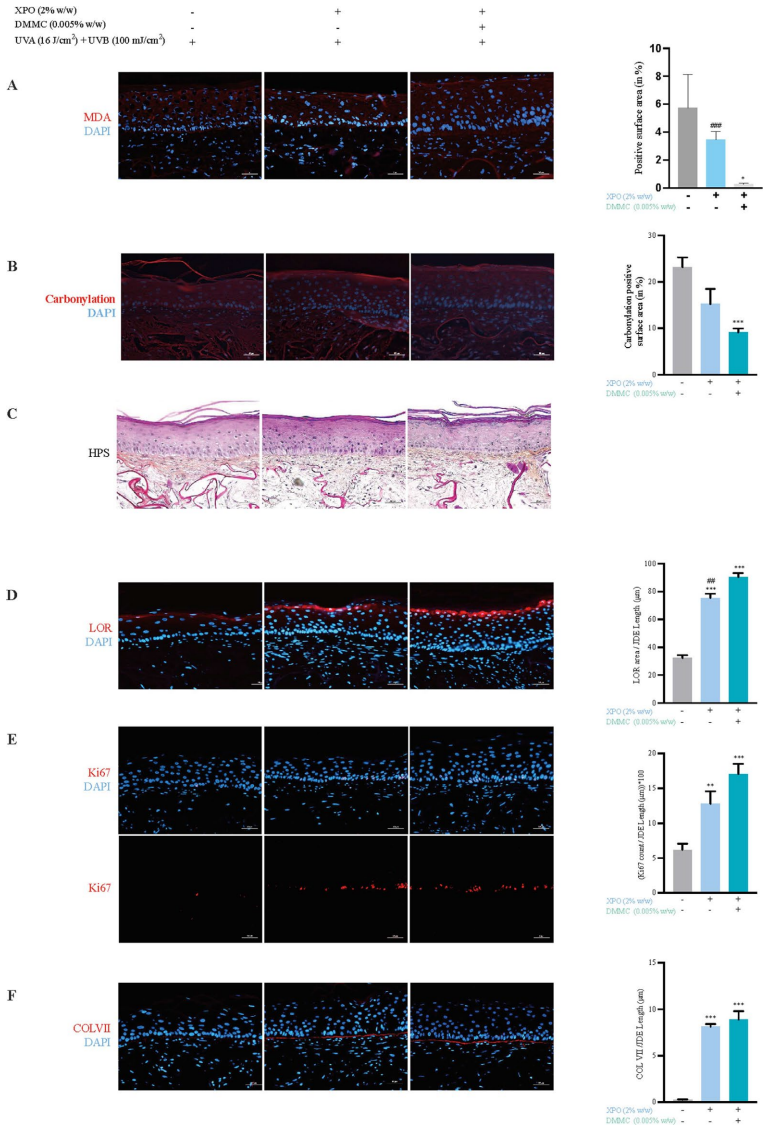

Figure 3. Combined effects of XPO and DMMC on oxidative damage and epidermal structure and DEJ integrity in UV-irradiated reconstructed pigmented human skin. Representative histological and immunofluorescence images of 3D reconstructed pigmented human skin models treated with 2% XPO or the combination of 2% XPO and 0.005% DMMC following UVA (16 J/cm^2) and UVB (100 mJ/cm^2) exposure. (A) Immunofluorescence staining for MDA (red) with nuclear counterstaining by DAPI (blue) illustrates lipid peroxidation damage. (B) Immunofluorescence staining for protein carbonylation (red) with nuclear counterstaining by DAPI (blue) illustrates protein oxidation damage. (C) HPS staining shows preserved epidermal and dermal architecture in treated groups. (D) Immunofluorescence staining for LOR (red) with nuclear counterstaining by DAPI (blue) illustrates epidermal differentiation. Quantitative analysis of LOR thickness (µm), (E) Immunofluorescence staining for Ki67 (red) with nuclear counterstaining by DAPI (blue) illustrates basal keratinocyte proliferation. Quantitative analysis of Ki67 positive cell density per DEJ length (/100 µm), and (F) Immunofluorescence staining for COL VII (red) with nuclear counterstaining by DAPI (blue) illustrates the DEJ. Quantitative analysis of COL VII deposition (µm). Data are presented as mean ± SEM (n = 3). Scale bar = 50 µm. Statistical significance: *$p < 0.05$, ***$p < 0.001$ vs. UVA + UVB-only group; $^{\#}p < 0.05$, $^{\#\#}p < 0.01$, $^{\#\#\#}p < 0.001$ vs. the combined XPO and DMMC treatment group.

Immunofluorescence staining for MDA and protein carbonylation evaluated the lipid and protein oxidation markers in the dermis after UV exposure. The combination of XPO/DMMC significantly reduced their levels, effectively mitigating UV induced oxidative damage (**Figure 3(A)**, **Figure 3(B)**). Epidermal homeostasis is related with differentiation, proliferation and dermal-epidermal junction (DEJ) integrity, immunofluorescence detection of LOR, Ki67 and COL VII revealed that XPO alone upregulated LOR and Ki67 expression versus the UV control, and co-treatment with DMMC further enhanced both markers to levels significantly higher than XPO monotherapy. COL VII expression was significantly increased in all treated groups, with no significant difference between XPO alone and the combination. Quantitative analysis also validated that XPO/DMMC combination markedly elevated LOR expression thickness, Ki67-positive cell density and COL VII deposition compared to the UV-irradiated control, and outperformed XPO monotherapy in multiple key endpoints (**Figure 3(D)**, **Figure 3(F)**). These data demonstrate that co-treatment delivers superior tissue-protective effects compared with single treatment and improve the recovery of epidermal regeneration and skin barrier function following UV damage.

3.5. Combined Application of XPO and DMMC Improves Wrinkle Appearance: A Clinical Hemi-Face Study

To confirm the anti-aging efficacy of XPO and DMMC in vivo, a double-blind, placebo-controlled, 28-day clinical hemi-face study was conducted in 33 Asian female subjects, aged 45 - 60 y.o., with skin phototypes II to IV. Participants applied a formulation containing 2% XPO and 0.05% DMMC to one side of the face and a placebo to the contralateral side. Both formulations were applied twice a day during the study period.

3D images of the underneath eye were acquired with PRIMOS (Canfield, USA). Quantitative analysis of the 3D images revealed that, after 28 days of treatment, the XPO and DMMC-treated side showed a significant reduction in wrinkle projection depth compared to both initial time and the placebo-treated side (**Figure 4**). Although a trend toward wrinkle reduction was observed at day 14 for the XPO and DMMC treatment, the effect reached statistical significance only on day 28. These clinical findings corroborate the *in vitro* and *ex vivo* data, supporting the efficacy of the XPO and DMMC combination in improving wrinkle depth.

4. Discussion

Environmental stressors such as UV radiation and pollution are key contributors to skin aging through mechanisms involving ROS, DNA damage, lipid and protein oxidation, and melanogenesis [18]-[21]. The present study demonstrates that DMMC and *Vigna angularis* seed extract, either in AZK or XPO exert distinct yet complementary protective effects across multiple skin layers, leading to functional and clinical improvements in skin exposed to photo-oxidative and pollutant stress.

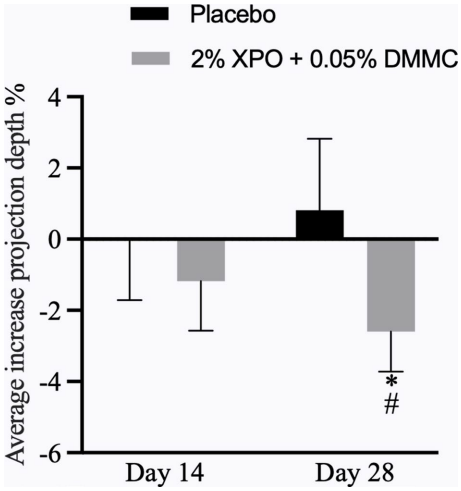

Figure 4. Clinical wrinkle improvement following combined application of XPO and DMMC. Bar graph showing changes in average wrinkle projection depth (%) at days 14 and 28 in hemi-faces treated with either the placebo or the formulation containing 2% XPO and 0.05% DMMC. Data are presented as mean ± SEM (n = 33). *p < 0.05 vs. placebo; #p < 0.05 vs. initial time (within group).

Both UVA and UVB radiation are well-established inducers of ROS generation, initiating a cascade of oxidative damage in the skin [22]. ROS contribute to lipid peroxidation, leading to the formation of reactive carbonyl species such as MDA. These carbonyl compounds can modify proteins through carbonylation, a hallmark of oxidative protein injury [23]. ROS also promote DNA strand breaks and oxidative base lesions in nucleic acids, including 8-oxodG and 8-OHG [6]. These processes represent key mechanistic pathways underlying extrinsic skin aging. ROS also promote the activation of matrix metalloproteases (MMPs), enzymes responsible for collagen degradation. This process compromises dermal integrity and contributes to visible signs of aging, such as wrinkle formation.

AZK, rich in antioxidant components, markedly decreased levels of 8-oxodG and 8-OHG in keratinocytes exposed to combined environmental stressors—including elevated temperature, CO_2, $PM_{2.5}$, and simulated solar radiation—underscoring its role in protecting against oxidative DNA and RNA damage. Additionally, its preserved form in solution, XPO, significantly reduced UV-induced protein carbonylation in reconstructed pigmented skin when combined with DMMC, suggesting effective mitigation of protein oxidative damage which may reflect either a reduction in lipid peroxidation-derived reactive carbonyl species or interference with the covalent modification of proteins by these intermediates.

DMMC exerted its protective effects through a dual antioxidant mechanism involving both direct free radical scavenging and transcriptional activation of intrinsic cellular defense pathways, as supported by both prior studies and the present findings. Previous reports have demonstrated that DMMC directly scavenges reactive species, including singlet oxygen and peroxynitrite—molecules implicated in UVA-induced photooxidative and nitrosative damage [14]. While these specific mechanisms were not evaluated in this study, our results demonstrate that

DMMC mitigated oxidative damage and promoted cell survival under multiple stress conditions.

Beyond its direct antioxidant effects, DMMC activated intrinsic cellular defense pathways. Transcriptomic profiling revealed significant upregulation of genes involved in redox homeostasis (e.g., GPX2, GCLC, SODs, PRDXs), glutathione metabolism, xenobiotic detoxification (e.g., CYP1A1, UGTs, GSTs), and efflux transport (e.g., ABCA4, ABCG1), suggesting activation of NRF2- and AHR-mediated transcriptional programs which mediate cellular adaptation to environmental stressors [24] [25]. These molecular adaptations likely contribute to DMMC's broader cytoprotective effects, including reduced genotoxicity in keratinocytes exposed to photoactivated pyrene, protection against UVA-induced DNA damage in melanocytes, attenuation of UVB-induced protein oxidation in fibroblasts, and inhibition of basal melanogenesis in melanocytes.

Pyrene is a representative polycyclic aromatic hydrocarbon (PAH) whose genotoxicity depends on photoactivation by UVA or visible light [26]. Upon activation, pyrene generates ROS that induce DNA strand breaks and oxidative genotoxicity [26]. In our study, DMMC significantly reduced DNA damage in keratinocytes exposed to photoactivated pyrene and in melanocytes exposed to UVA. It also attenuated UVB-induced protein oxidation in fibroblasts and improved their viability under H_2O_2-induced oxidative stress, further confirming its broad cytoprotective role. These protective effects strongly support the conclusion that DMMC reduces genotoxicity primarily through its antioxidant action.

Notably, the DNA-protective effect of DMMC was more pronounced under UVA than UVB irradiation. While DMMC significantly mitigated UVA-induced DNA strand breaks, it showed minimal protection against UVB-induced genotoxicity. This observation aligns with the differential absorption characteristics of UV wavelengths: UVB is directly absorbed by DNA and induces strand breaks at relatively low doses, whereas UVA exerts its genotoxic effects primarily through ROS generation [27]. Thus, DMMC's DNA-protecting efficacy under UVA, but not UVB, is consistent with its antioxidant-driven mode of action.

In addition to their antioxidative and genoprotective functions, both XPO and DMMC exhibited inhibitory effects on melanogenesis. XPO reduced UV-induced melanin accumulation in reconstructed pigmented skin, indicating suppression of UV-stimulated pigment production. DMMC significantly decreased baseline melanin content in normal human melanocytes, even in the absence of pigment-inducing stimuli, suggesting that it may influence melanogenic pathways—potentially through mechanisms linked to oxidative stress. These anti-melanogenic effects are particularly relevant for improving pigmentation uniformity and mitigating hyperpigmentation associated with photoaging, thereby further extending the cosmetic utility of both compounds.

The combination of XPO and DMMC improved markers of epidermal regeneration and dermal-epidermal cohesion to a greater degree than individual treatment. The observed enhancement in LOR expression suggests restoration of ter-

minal epidermal differentiation, a critical process for barrier formation and resilience [28] [29]. The increase in Ki67-positive basal keratinocytes indicates stimulation of epidermal renewal, reflecting improved regenerative potential under UV-damaged conditions. Furthermore, upregulation of COL VII—a structural anchor of the DEJ—suggests reinforcement of tissue architecture and mechanical cohesion [30]. These findings support the hypothesis that XPO and DMMC, particularly in combination, not only mitigate oxidative stress but also promote structural repair.

These mechanistic findings translated into meaningful clinical outcomes. In a 28-day placebo-controlled hemi-face study, application of the XPO and DMMC combination significantly reduced wrinkle depth compared to placebo. This clinical improvement aligns with observed enhancements in barrier integrity, dermal-epidermal cohesion, and oxidative stress reduction, and validates the predictive value of the *in vitro* and *ex vivo* models employed.

Altogether, the combined use of XPO and DMMC offers a rational and comprehensive strategy for targeting multiple facets of environmentally induced skin aging. XPO provides rapid protection by directly mitigating oxidative damage and preserving genomic stability. DMMC, through its dual antioxidant mechanism, offers both immediate free radical scavenging and long-term enhancement of cellular defense, detoxification, and structural resilience. Dual treatment with XPO and DMMC acts on oxidative, structural and genomic pathways at the same time. Their multi-layer protective profiles support their use in dermocosmetics targeting UV-triggered photoaging, whereas protection against pollutant damage has not been confirmed in human clinical assessments.

5. Conclusion

In conclusion, this study demonstrates that DMMC and *Vigna angularis* seed extract, either in AZK or XPO provide complementary and protection against environmentally induced skin aging. *Vigna angularis* seed extract acts rapidly to mitigate oxidative damage and maintain genomic stability, while DMMC combines direct antioxidant activity with transcriptional activation of cellular defense and structural repair pathways. Together, they protect from oxidative damage and improve epidermal regeneration, dermal-epidermal cohesion, pigmentation balance, and clinical wrinkle reduction. These findings highlight the value of including these ingredients in advanced skincare formulations designed to address multiple pathways involved in photoaging and pollution-induced skin damage. Such formulations can help protect and rejuvenate the skin by counteracting various environmental stressors and promoting overall skin health.

Data Availability Statement

Regarding data availability, all data generated or analysed during this study are included in this published article. Full unprocessed raw microarray outputs and original clinical source records are archived by Lubrizol Life Science and contain

confidential proprietary information protected by internal confidentiality agreements. These raw datasets cannot be publicly uploaded as supplementary files. Qualified researchers may contact the corresponding author by email to submit a reasonable request for access to raw data for non-commercial academic use only.

Ethical Statement

This clinical study (approval code: HSRB-24-015) was conducted in accordance with the ethical principles of the Declaration of Helsinki and approved by the Human Subject Research Board (HSRB) of Lubrizol Life Science. All test materials, including the active formulation (2% Xpozuki biotech ingredient LA and 0.05% Lipochroman) and placebo emulsion, were composed of ingredients with prior HSRB approval for leave-on cosmetic use (see **Appendix** Table in the HSRB application HSRB-24-015 for ingredient-sepcific HSRB approval details).

A total of 33 female Chinese volunteers aged 45 - 60 years (with self-reported wrinkles, dullness, and sallowness) were enrolled in this 28-day split-face trial. Prior to study initiation, all participants were fully informed of the study objectives, procedures, potential risks, and benefits, and provided written informed consent. The study complied with relevant cosmetic regulations in China, where the product is classified as a cosmetic and exempt from pre-approval by regulatory authorities. All data were collected and analyzed anonymously to protect participant privacy.

Acknowledgements

This study was funded by Lubrizol Life Science. The authors wish to thank Labskin Creations for conducting the *in vitro* assay in the 3D skin models.

Author Contributions

JW conceived and designed the study under supervision of CCZ. MV, CG, GM, EG, MQ and JC performed the experiments, collected and analyzed the data, and conducted statistical analysis. JW, MJY, and QL contributed to the interpretation of the results. JW and CCZ wrote the initial draft of the manuscript. All authors read and approved the final version of the manuscript.

Conflicts of Interest

The authors declare no conflicts of interest regarding the publication of this paper.

References

[1] Pillai, S., Oresajo, C. and Hayward, J. (2005) Ultraviolet Radiation and Skin Aging: Roles of Reactive Oxygen Species, Inflammation and Protease Activation, and Strategies for Prevention of Inflammation-induced Matrix Degradation—A Review. *International Journal of Cosmetic Science*, **27**, 17-34. https://doi.org/10.1111/j.1467-2494.2004.00241.x

[2] Serre, C., Busuttil, V. and Botto, J.M. (2018) Intrinsic and Extrinsic Regulation of Human Skin Melanogenesis and Pigmentation. *International Journal of Cosmetic Science*, **40**, 328-347. https://doi.org/10.1111/ics.12466

[3] Ali, A., Khan, H., Bahadar, R., Riaz, A. and Asad, M.H.H.B. (2020) The Impact of Airborne Pollution and Exposure to Solar Ultraviolet Radiation on Skin: Mechanistic and Physiological Insight. *Environmental Science and Pollution Research*, **27**, 28730-28736. https://doi.org/10.1007/s11356-020-09280-4

[4] Grether-Beck, S., Felsner, I., Brenden, H., Marini, A., Jaenicke, T., Aue, N., *et al.* (2021) Air Pollution-Induced Tanning of Human Skin. *British Journal of Dermatology*, **185**, 1026-1034. https://doi.org/10.1111/bjd.20483

[5] Wei, M., He, X., Liu, N. and Deng, H. (2024) Role of Reactive Oxygen Species in Ultraviolet-Induced Photodamage of the Skin. *Cell Division*, **19**, Article No. 1. https://doi.org/10.1186/s13008-024-00107-z

[6] Cadet, J., Douki, T. and Ravanat, J. (2015) Oxidatively Generated Damage to Cellular DNA by UVB and UVA Radiation. *Photochemistry and Photobiology*, **91**, 140-155. https://doi.org/10.1111/php.12368

[7] de Jager, T.L., Cockrell, A.E. and Du Plessis, S.S. (2017) Ultraviolet Light Induced Generation of Reactive Oxygen Species. In: Ahmad, S.I., Ed., *Ultraviolet Light in Human Health, Diseases and Environment*, Springer International Publishing, 15-23. https://doi.org/10.1007/978-3-319-56017-5_2

[8] Dalle-Donne, I., Rossi, R., Giustarini, D., Milzani, A. and Colombo, R. (2003) Protein Carbonyl Groups as Biomarkers of Oxidative Stress. *Clinica Chimica Acta*, **329**, 23-38. https://doi.org/10.1016/s0009-8981(03)00003-2

[9] Pirincciogluu, A.G., Gökalp, D., Pirincciogluu, M., Kizil, G. and Kizil, M. (2010) Malondialdehyde (MDA) and Protein Carbonyl (PCO) Levels as Biomarkers of Oxidative Stress in Subjects with Familial Hypercholesterolemia. *Clinical Biochemistry*, **43**, 1220-1224. https://doi.org/10.1016/j.clinbiochem.2010.07.022

[10] Li, C.S., Wu, K.Y., Chang-Chien, G.P. and Chou, C.C. (2005) Analysis of Oxidative DNA Damage 8-Hydroxy-2'-Deoxyguanosine as a Biomarker of Exposures to Persistent Pollutants for Marine Mammals. *Environmental Science & Technology*, **39**, 2455-2460. https://doi.org/10.1021/es0487123

[11] Chiorcea-Paquim, A.M. (2022) 8-Oxoguanine and 8-Oxodeoxyguanosine Biomarkers of Oxidative DNA Damage: A Review on HPLC–ECD Determination. *Molecules*, **27**, Article No. 1620. https://doi.org/10.3390/molecules27051620

[12] Gülden, M., Jess, A., Kammann, J., Maser, E. and Seibert, H. (2010) Cytotoxic Potency of H_2O_2 in Cell Cultures: Impact of Cell Concentration and Exposure Time. *Free Radical Biology and Medicine*, **49**, 1298-1305. https://doi.org/10.1016/j.freeradbiomed.2010.07.015

[13] Chaudhuri, R.K., Meyer, T., Premi, S. and Brash, D. (2020) Acetyl Zingerone: An Efficacious Multifunctional Ingredient for Continued Protection against Ongoing DNA Damage in Melanocytes after Sun Exposure Ends. *International Journal of Cosmetic Science*, **42**, 36-45. https://doi.org/10.1111/ics.12582

[14] Nonell, S., García-Díaz, M., Viladot, J.L. and Delgado, R. (2013) Singlet Molecular Oxygen Quenching by the Antioxidant Dimethylmethoxy Chromanol in Solution and in *ex Vivo* Porcine Skin. *International Journal of Cosmetic Science*, **35**, 272-280. https://doi.org/10.1111/ics.12039

[15] Oh, S., Zheng, S., Fang, M., Kim, M., Bellere, A.D., Jeong, J., *et al.* (2023) Anti-Photoaging Effect of *Phaseolus angularis* L. Extract on UVB-Exposed HaCaT Keratinocytes and Possibilities as Cosmetic Materials. *Molecules*, **28**, Article No. 1407. https://doi.org/10.3390/molecules28031407

[16] Tian, S., Chen, S., Feng, Y. and Li, Y. (2021) The Interactions of Small Proline-Rich Proteins with Late Cornified Envelope Proteins Are Involved in the Pathogenesis of

Psoriasis. *Clinical, Cosmetic and Investigational Dermatology*, **14**, 1355-1365. https://doi.org/10.2147/ccid.s336072

[17] Zhang, C., Hu, Z., Lone, A.G., Artami, M., Edwards, M., Zouboulis, C.C., *et al.* (2022) Small Proline-Rich Proteins (SPRRs) Are Epidermally Produced Antimicrobial Proteins That Defend the Cutaneous Barrier by Direct Bacterial Membrane Disruption. *eLife*, **11**, e76729. https://doi.org/10.7554/elife.76729

[18] Watson, R.E.B., Gibbs, N.K., Griffiths, C.E.M. and Sherratt, M.J. (2014) Damage to Skin Extracellular Matrix Induced by UV Exposure. *Antioxidants & Redox Signaling*, **21**, 1063-1077. https://doi.org/10.1089/ars.2013.5653

[19] Panich, U., Sittithumcharee, G., Rathviboon, N. and Jirawatnotai, S. (2016) Ultraviolet Radiation-Induced Skin Aging: The Role of DNA Damage and Oxidative Stress in Epidermal Stem Cell Damage Mediated Skin Aging. *Stem Cells International*, **2016**, Article ID: 7370642. https://doi.org/10.1155/2016/7370642

[20] Burke, K.E. (2018) Mechanisms of Aging and Development—A New Understanding of Environmental Damage to the Skin and Prevention with Topical Antioxidants. *Mechanisms of Ageing and Development*, **172**, 123-130. https://doi.org/10.1016/j.mad.2017.12.003

[21] Parrado, C., Mercado-Saenz, S., Perez-Davo, A., Gilaberte, Y., Gonzalez, S. and Juarranz, A. (2019) Environmental Stressors on Skin Aging. Mechanistic Insights. *Frontiers in Pharmacology*, **10**, Article No. 759. https://doi.org/10.3389/fphar.2019.00759

[22] Widel, M., Krzywon, A., Gajda, K., Skonieczna, M. and Rzeszowska-Wolny, J. (2014) Induction of Bystander Effects by UVA, UVB, and UVC Radiation in Human Fibroblasts and the Implication of Reactive Oxygen Species. *Free Radical Biology and Medicine*, **68**, 278-287. https://doi.org/10.1016/j.freeradbiomed.2013.12.021

[23] Estévez, M., Padilla, P., Carvalho, L., Martín, L., Carrapiso, A. and Delgado, J. (2019) Malondialdehyde Interferes with the Formation and Detection of Primary Carbonyls in Oxidized Proteins. *Redox Biology*, **26**, Article ID: 101277. https://doi.org/10.1016/j.redox.2019.101277

[24] Dietrich, C. (2016) Antioxidant Functions of the Aryl Hydrocarbon Receptor. *Stem Cells International*, **2016**, Article ID: 7943495. https://doi.org/10.1155/2016/7943495

[25] Robertson, H., Dinkova-Kostova, A.T. and Hayes, J.D. (2020) NRF2 and the Ambiguous Consequences of Its Activation during Initiation and the Subsequent Stages of Tumourigenesis. *Cancers*, **12**, Article No. 3609. https://doi.org/10.3390/cancers12123609

[26] Botta, C., Di Giorgio, C., Sabatier, A. and De Méo, M. (2009) Effects of UVA and Visible Light on the Photogenotoxicity of Benzo[a]pyrene and Pyrene. *Environmental Toxicology*, **24**, 492-505. https://doi.org/10.1002/tox.20455

[27] Budden, T. and Bowden, N. (2013) The Role of Altered Nucleotide Excision Repair and UVB-Induced DNA Damage in Melanomagenesis. *International Journal of Molecular Sciences*, **14**, 1132-1151. https://doi.org/10.3390/ijms14011132

[28] Nithya, S., Radhika, T. and Jeddy, N. (2015) Loricrin—An Overview. *Journal of Oral and Maxillofacial Pathology*, **19**, 64-68. https://doi.org/10.4103/0973-029x.157204

[29] Ishitsuka, Y. and Roop, D.R. (2020) Loricrin: Past, Present, and Future. *International Journal of Molecular Sciences*, **21**, Article No. 2271. https://doi.org/10.3390/ijms21072271

[30] Conradt, G., Hausser, I. and Nyström, A. (2024) Epidermal or Dermal Collagen VII Is Sufficient for Skin Integrity: Insights to Anchoring Fibril Homeostasis. *Journal of Investigative Dermatology*, **144**, 1301-1310.e7. https://doi.org/10.1016/j.jid.2023.11.003

Appendix: Table in the HSRB Application HSRB-24-015 for Ingredient-Specific HSRB Approval Details

Inter Office Memo
Date: 1-July-2024
To: Cindy Sullivan
cc: Sharon Qu, Gemma Mola, Raquel Delgado,
From: Susie Jin, Melanie Qiao REF: HSRB-24-015
Subject: Lipochroman and Xpozuki in-vivo test

Lubrizol Safety SOP Outline:

1) The rationale and objective of the study.
2) Alternative approaches.
3) Applicable regulations governing the ingredient, the finished product and the testing process for the jurisdiction in which the testing will take place.
4) The identity of the test material.
5) The existing information on the hazards of the test material.
6) Sample storage requirements including stability.
7) The identity of the test subjects.
8) The methodology for conducting the study, including test material administration, observations of effects/responses, data analyses, etc.

1. Rationale and Objective:

The oxidative stress resistance from the combination of Dimethylmethoxy Chromanol (Lipochroman) and natural peptides derived from red beans (Xpozuki) have been evaluated on the novel full-thickness pigmented skin model. Paper published in 2023 IFSCC showed significantly improvement for whole skin structural health. This study will evaluate the active combination clinical performance on Chinese volunteers.

For this project, two emulsions will be developed in one group of volunteers for semi-face test, one placebo emulsion, one containing 2% Xpozuki and 0.05% Lipochroman.

2. Alternative Approaches:

At this point there are no alternatives.

3. Applicable Regulations:

This product is classified as a cosmetic product in China. No pre-approval by regulatory authorities is required.

4. Identity of the Test Materials:

For this project, two emulsions will be developed, one placebo emulsion, one containing 2% Xpozuki and 0.05% Lipochroman.

One cleanser with no specific efficacy will be used for wash-up and will be used

during the test period. See details below:

https://www.za-cosmetics.com/Products/Detail.aspx?Id=39 (Za Facial Cleansing Foam)

The formulations and ingredients used for the clinical trial are listed in **Table A1**:

Table A1. Emulsion formulations and ingredients.

No.	Trade Name	Active formula wt.%	Placebo formula wt.%	Function	INCI Name	Max HSRB Approved wt.%
1	DI Water	q.s. 100%	q.s. 100%	Diluent	DI Water	-
2	Disodium EDTA	0.05	0.05	Chelating agent	Disodium EDTA	HSRB-16-026 Leave on 0.2%
3	SymSave® H	0.50	0.50	Preservative	Hydroxyacetophenone	HSRB-20-021 Leave on 0.5%
4	Hydrolite® 6	0.50	0.50	Preservative	1,2-Hexanediol	HSRB-19-010 Leave on 2%
5	Butylene glycol	2.00	2.00	Humectant	Butylene glycol	HSRB-17-008 Leave on 5%
6	Pemulen™ EZ-4U	0.50	0.50	Rheology modifier	Acrylates/C10-30 Alkyl Acrylate Crosspolymer	HSRB-17-015 Leave on 0.5%
7	Schercemol DIS	3.00	3.00	Emollient	Diisopropyl Sebacate	HSRB-22-017 Leave on 9%
8	AMP-ULTRA® PC 2000	0.20 PH 5.0 - 5.5	0.20 PH 5.0 - 5.5	PH adjuster	Aminomethyl propanol (95%)	HSRB-07-003 (Fixate tradeshow) Leave on 2%
9	Xpozuki biotech ingredient LA	2.00	/	Active	WATER (AQUA), GLYCERIN, LEUCONOSTOC/RADISH ROOT FERMENT FILTRATE, PHASEOLUS ANGULARIS SEED EXTRACT, CITRIC ACID, LEVULINIC ACID, SODIUM LEVULINATE	HSRB-21-007 Leave on 2%
10	Lipochroman	0.05	/	Active	Dimethylmethoxy chromanol	HSRB-19-009 Leave on 0.05%
11	SODIUM METABISULFITE	0.03	0.03	Antioxidant agent	SODIUM METABISULFITE	HSRB-21-013 Leave on 0.25% (wash off after evaluation completed)

Formula pH is ~5.0 - 5.5.

5. Hazards of Test Materials:

All ingredients are used within levels and exposure period previously approved by HSRB (See list at: http://amersp.lubrizol.com/sites/NCS/SiteDirectory/PHCRegulatory/Human%20Subject%20Testing%20Studies/1HSRB%20approved%20materials.xls?Web=1)

6. Storage Requirements and Stability:

Samples will be prepared in Skin Essential Applications (Shanghai Song Jiang, China), and cleanser is the commercial product: Za Facial Cleansing Foam. The study will be performed in China in vivo lab (Shanghai). Samples will be stored under room temperature. In both cases panelists will take product samples home and they will follow instructions of application daily.

7. Identity of Test Subjects:

The test is designed as half face test. At least 30 panelists will be recruited. These panelists will be from 45 - 60 years old female, currently claim to have some signs of wrinkle and dull & sallow. Application period is 28 days.

Table A2. Genes upregulated by DMMC treatment in HEKa.

Gene Category	Gene Symbol	Gene Name	% Fold-change
Epidermal Barrier	SPRR1A	Small proline-rich protein 1A	189.3
Epidermal Barrier	SPRR1B	Small proline-rich protein 1B	187.8
Epidermal Barrier	SPRR2E	Small proline-rich protein 2E	92.1
Epidermal Barrier	SPRR2G	Small proline-rich protein 2G	29.9
Antioxidant & Redox Homeostasis	PGD	phosphogluconate dehydrogenase	289.7
Antioxidant & Redox Homeostasis	G6PD	glucose-6-phosphate dehydrogenase	177.2
Antioxidant & Redox Homeostasis	PRDX2	peroxiredoxin 2	23.7
Antioxidant & Redox Homeostasis	PRDX1	peroxiredoxin 1	64.5
Antioxidant & Redox Homeostasis	PRDX5	peroxiredoxin 5	33.8
Antioxidant & Redox Homeostasis	SOD3	superoxide dismutase 3, extracellular	61.3
Antioxidant & Redox Homeostasis	SOD2	superoxide dismutase 2, mitochondrial	37.2
Antioxidant & Redox Homeostasis	GPX4	glutathione peroxidase 4	37.0
Antioxidant & Redox Homeostasis	GPX3	glutathione peroxidase 3	88.5
Antioxidant & Redox Homeostasis	GPX2	glutathione peroxidase 2	453.3
Antioxidant & Redox Homeostasis	GSR	glutathione reductase	123.9
Antioxidant & Redox Homeostasis	GCLM	glutamate-cysteine ligase, modifier subunit	221.7
Antioxidant & Redox Homeostasis	GCLC	glutamate-cysteine ligase, catalytic subunit	526.8
Xenobiotic Metabolism & Efflux	CYP1A1	cytochrome P450, family 1, subfamily A, polypeptide 1	539.1
Xenobiotic Metabolism & Efflux	CYP1B1	cytochrome P450, family 1, subfamily B, polypeptide 1	1910.4

Continued

Xenobiotic Metabolism & Efflux	SULT1A1	sulfotransferase family, cytosolic, 1A, member 1	51.5
Xenobiotic Metabolism & Efflux	SULT2B1	sulfotransferase family, cytosolic, 2B, member 1	327.8
Xenobiotic Metabolism & Efflux	UGT1A8	UDP glucuronosyltransferase 1 family, polypeptide A8	128.4
Xenobiotic Metabolism & Efflux	UGT1A6	UDP glucuronosyltransferase 1 family, polypeptide A6	79.0
Xenobiotic Metabolism & Efflux	GSTA4	glutathione S-transferase alpha 4	79.7
Xenobiotic Metabolism & Efflux	GSTM1	glutathione S-transferase mu 1	92.2
Xenobiotic Metabolism & Efflux	GSTM2	glutathione S-transferase mu 2	73.5
Xenobiotic Metabolism & Efflux	GSTM3	glutathione S-transferase mu 3	91.0
Xenobiotic Metabolism & Efflux	GSTM4	glutathione S-transferase mu 4	99.9
Xenobiotic Metabolism & Efflux	ABCA4	ATP-binding cassette, sub-family A, member 4	73.6
Xenobiotic Metabolism & Efflux	ABCC1	ATP-binding cassette, sub-family C, member 1	64.0
Xenobiotic Metabolism & Efflux	ABCG1	ATP-binding cassette, sub-family G, member 1	58.0